ADVANCED MATERIALS INTERFACES
www.advmatinterfaces.de

Multifunctional POSS-Based Nano-Photo-Initiator for Overcoming the Oxygen Inhibition of Photo-Polymerization and for Creating Self-Wrinkled Patterns

*Honghao Hou, Yanchang Gan, Jie Yin, and Xuesong Jiang**

Oxygen inhibition remains a challenge in photo-curing technology despite the expenditure of considerable effort in developing a convenient, efficient, and low-cost prevention method. Here, a novel strategy to prevent oxygen inhibition is presented; it is based on the self-assembly of multifunctional nano-photo-initiators (F_2-POSS-$(SH)_4$-TX/EDB) at the interface of air and the liquid monomer. These nano-photo-initiators consist of a thiol-containing polyhedral oligomeric silsesquioxane (POSS) skeleton onto which fluorocarbon chains and thioxanthone and dimethylaminobenzoate (TX/EDB) photo-initiator moieties are grafted. Real-time Fourier-transform infrared spectroscopy (FT-IR) is used to investigate the photo-polymerization of various acrylate monomers that are initiated by F_2-POSS-$(SH)_4$-TX/EDB and its model analogues in air and in N_2. FT-IR results show that F_2-POSS-$(SH)_4$-TX/EDB decreases the effects of oxygen inhibition. X-ray photo-electron spectroscopy and atomic force microscopy reveal that the self-assembly of F_2-POSS-$(SH)_4$-TX/EDB at the air/(liquid monomer) interface forms a cross-linked top layer via thiol–ene polymerization; this layer acts as a physical barrier against the diffusion of oxygen from the surface into the bulk layer. A mismatch in the shrinkage between the top and bulk layers arise as a result of the different types of photo-cross-linking reactions. Subsequently, the surface develops a wrinkled pattern with a low surface energy. This strategy exhibits considerable potential for preventing oxygen inhibition, and the wrinkled pattern may prove very useful in photo-curing technology.

1. Introduction

Free radical photo-polymerization is widely used in many fields,[1] including coatings,[2] microelectronics,[3] photoresists,[4] and dental materials.[5] This is because the process offers obvious advantages over other polymerization processes in terms of energy savings, being environmentally friendly, time savings, low cost, ambient temperature requirements, and spatial and temporal control.[1–3,6,7] However, a primary challenge that is encountered in free radical photo-polymerization is oxygen inhibition, which limits the wide application of the process.[8–22] Molecular oxygen is known to inhibit photo-polymerization by reacting with active radicals to form much more stable peroxy radicals that cannot reinitiate polymerization. Generally, free radical polymerization is inhibited by oxygen dissolved within the monomers and oxygen that diffuses from the surrounding air into the systems being photo-cured.[8,10] For photo-polymerization in thin films, the inhibitory effect becomes especially pronounced for a sample that is exposed to air because of the diffusion of oxygen from the air into the sample. The sample cannot be photo-cured completely, and the top layer becomes tacky because oxygen inhibits surface polymerization. Therefore, oxygen inhibition negatively impacts the polymerization kinetics as well as the structure and performance of the resulting polymer.

Both chemical and physical approaches have been developed to overcome this considerable challenge of oxygen inhibition. Chemical methods include the introduction of additives that can rapidly consume O_2, such as amines,[11] thiols,[12–15] organoboranes,[16] organosilanes,[17] and singlet oxygen scavengers;[18] the development of low-oxygen-sensitive monomers and oligomers;[19] and the exploitation and utilization of functional photo-initiators.[20] For example, additives of amines, thiols, and triphenylphosphates can scavenge and transform peroxy radicals into active radicals to initiate polymerization.[1,2,10] Nie and co-workers exploited the low surface energy of fluorinated carbon chains and demonstrated that the aggregation of 2-methyl-2-benzoylethanolpentadecafluorooctanoate (1173-F) on the top surface of a sample can reduce oxygen inhibition.[21] These creative chemical methods enable the polymerization process to overcome inhibition from dissolved oxygen, but they do not efficiently reduce inhibition from diffused oxygen. Physical approaches to counter oxygen surface inhibition include increasing the light intensity to create an inert atmosphere and the use of physical barriers that are impermeable to oxygen.[1,10] Protecting the surface by

Dr. H. H. Hou, Dr. Y. C. Gan, Prof. J. Yin, Prof. X. S. Jiang
School of Chemistry and Chemical Engineering
State Key Lab of Metal Matrix Composite Materials
Shanghai Jiao Tong University
Shanghai 200240, P. R. China
Tel.:+86–21–54743268
Fax: +86–21–54747445
E-mail: ponygle@sjtu.edu.cn

DOI: 10.1002/admi.201400385

encapsulation in an inert atmosphere (e.g., N_2, Ar, CO_2)[1,10,22] and using physical barriers (PVA/PET [poly(vinyl alcohol)/poly(ethylene terephthalate)], paraffin oil, or other materials)[1,10] can very efficiently restrict the access of molecular oxygen, thereby reducing the inhibitory effect of oxygen diffusion from the surroundings. However, it is inconvenient and costly to use an inert atmosphere and physical barriers in practical applications.

Very recently, we found that thiol-containing polyhedral oligomeric silsesquioxane grafted with fluorocarbon chains ("F-POSS-SH") self-assembled at the interface of air with an acrylate liquid resin, forming a top layer that was cured via oxygen-insensitive thiol–ene photo-polymerization.[23] This result motivated us to investigate whether a thiol–ene photo-cross-linked top layer could serve as a self-generating physical barrier against oxygen diffusion, thereby reducing oxygen inhibition. Thus, we developed a multi-functional photo-initiator based on POSS, which consists of fluorocarbon chains, thiol groups, and photo-initiator moieties. We found that oxygen inhibition could be dramatically reduced using this multi-functional nano-photo-initiator. The entire strategy is illustrated in **Scheme 1**. Fluorocarbon chains containing a nano-photo-initiator self-assembled in the top layer. Oxygen-insensitive thiol–ene photo-polymerization[12–15,24] and a high concentration of the photo-initiator moiety resulted in the curing of the top layer by UV irradiation even when the sample was exposed to air. The photo-cured self-assembled top layer served as a physical barrier against the diffusion of oxygen from the air into the sample. Thus, conventional radical photo-polymerization was able to progress smoothly in the lower bulk layer, and the inhibitory effect of oxygen was efficiently suppressed. Moreover, a mismatch in the shrinkage and mechanical properties between the top and bulk layers due to the different types of photo-cross-linking reactions resulted in a wrinkled pattern.

2. Results and Discussion

Thiol–halogen click chemistry was used to graft the functional moieties of the fluorocarbon chains (F), photo-initiator thioxanthone (TX), and co-initiator dimethylaminobenzoate (EDB) to mercaptopropyl-polysilsesquioxane (POSS-$(SH)_8$), in order to obtain the nano-photo-initiator (F_2-POSS-$(SH)_4$-TX/EDB), whose structure is shown in Scheme 1. For reference purposes, the detailed synthesis and structural characterization of F_2-POSS-$(SH)_4$-TX/EDB and its model photo-initiators can be found in the Supporting Information (SI: Figure S1–S6). The F_2-POSS-$(SH)_4$-TX/EDB exhibited the characteristic UV–vis absorption of thioxanthone, which indicated that TX had been successfully grafted to the POSS skeleton (Figure S7, SI). We considered a variety of physical and chemical features in designing a multi-functional POSS-based nano-photo-initiator. POSS is the smallest cubic silica nanoparticle that can be precisely defined, and it was chosen as the skeletal material to impart excellent mechanical and thermal properties to the resulting materials.[25] Fluorinated carbon chains were introduced to provide a low surface energy for the nano-photo-initiator, which is the key factor for the self-assembly of nano-photo-initiators in the top layer. TX and EDB were chosen as the photo-initiating moieties. TX has a high photo-initiation efficiency and adsorption characteristics near UV–vis range; it has thus been widely used as a hydrogen-abstraction photo-initiator in the presence of a co-initiator amine.[26] The physical mixture of TX and EDB constitutes the two-component

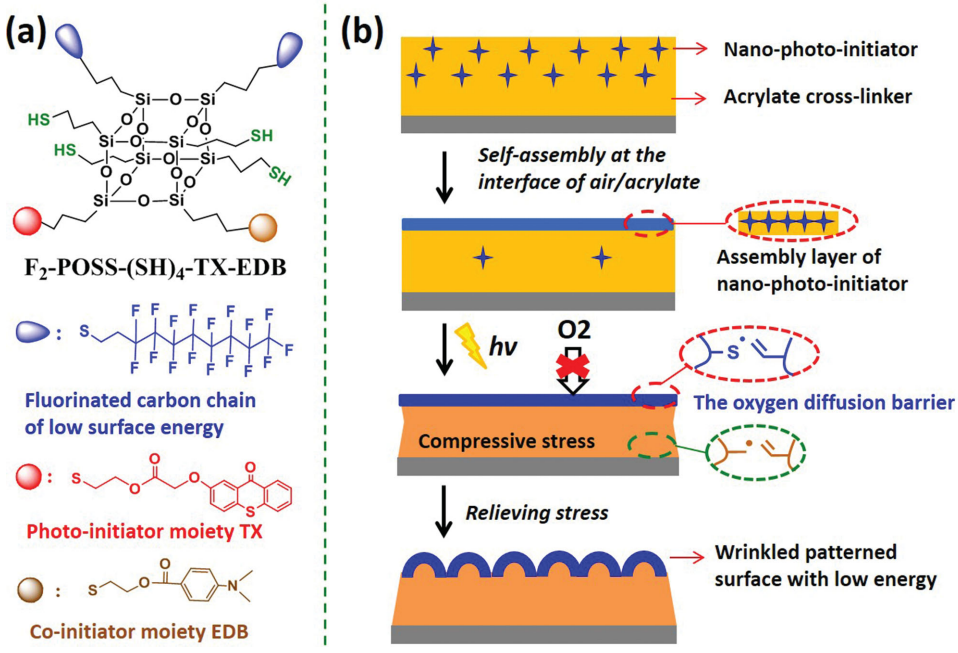

Scheme 1. a) Chemical structure of multi-functional POSS-based nano-photo-initiator F_2-POSS-$(SH)_4$-TX/EDB. b) Complete strategy for self-assembly of F_2-POSS-$(SH)_4$-TX/EDB at the interface of air and the monomer liquid, enabling the reduction of oxygen inhibition and creating the self-wrinkled pattern.

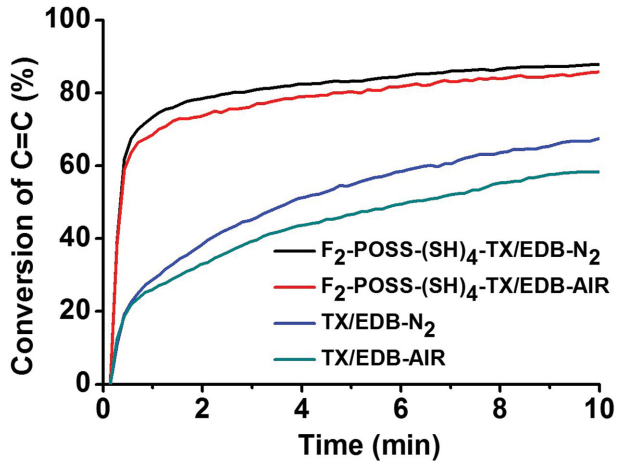

Figure 1. Real-time FT-IR investigation of photo-polymerization kinetics of A-BPE-10 using F_2-POSS-$(SH)_4$-TX/EDB and TX/EDB as photo-initiators in air or in N_2; the concentrations of all photo-initiators were 0.0248 M in terms of the TX moiety, and the light intensity was 3 mW cm^{-2}.

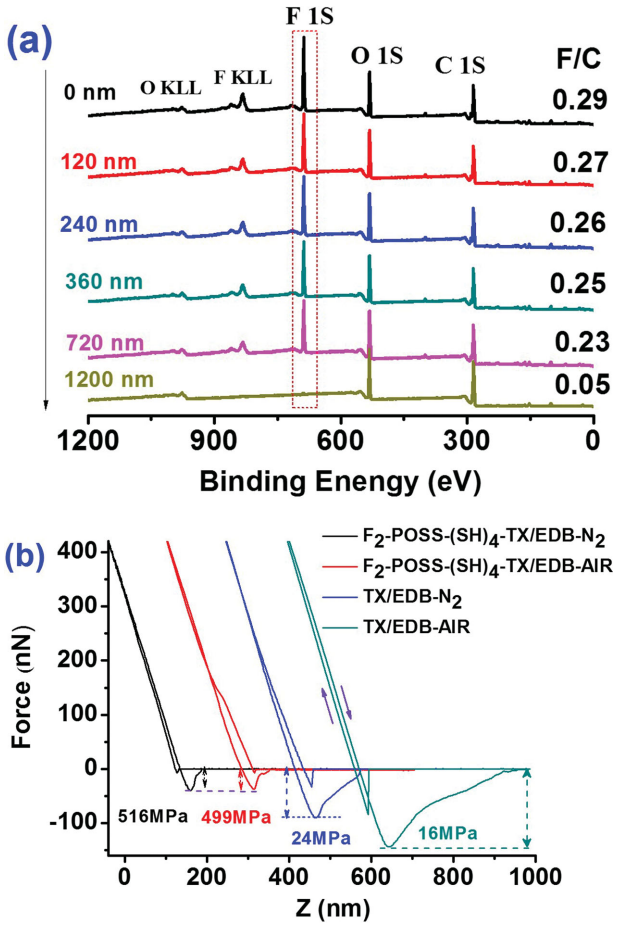

Figure 2. a) XPS spectra, showing depth-dependence of photo-cured A-BPE-10 film using F_2-POSS-$(SH)_4$-TX/EDB as a photo-initiator. b) AFM force curves of photo-cured A-BPE-10 films using F_2-POSS-$(SH)_4$-TX/EDB and TX/EDB as photo-initiators in N_2 and in air; the concentration of all of the photo-initiators was 0.0248 M in terms of the TX moiety; the UV light intensity was 3 mW cm^{-2}, and the exposure time was 10 min.

photo-cleavable photo-initiator (labeled as TX/EDB). The TX/EDB photo-initiating system is less sensitive to oxygen inhibition than a classical photo-cleavable photo-initiator because the amine EDB can transform stable peroxy radicals into active radicals to re-initiate polymerization.[10] The residual thiol moieties of F_2-POSS-$(SH)_4$-TX/EDB can participate in thiol–ene radical-mediated polymerization, which is known to be insensitive to oxygen inhibition.[24]

Scheme 1 shows the proposed mechanism for the use of F_2-POSS-$(SH)_4$-TX/EDB as a photo-initiator to reduce the inhibitory effect of oxygen. To test its ability to reduce oxygen inhibition, we used real-time Fourier-transform infrared spectroscopy (FT-IR) to study the photo-polymerization kinetics of ethoxylated bisphenol A diacrylate (A-BPE-10), which could be initiated by F_2-POSS-$(SH)_4$-TX/EDB in air and in N_2. A small-molecule model photo-initiator TX/EDB was also tested to serve as a reference. **Figure 1** shows almost identical kinetic curves for the photo-polymerization of A-BPE-10 when initiated by F_2-POSS-$(SH)_4$-TX/EDB in air and in N_2; thus, there was no obvious inhibitory effect by oxygen. The final double-bond (C = C) conversion in this photo-polymerization of A-BPE-10 was as high as 85.3% successful when the sample was exposed to air, which was slightly less than the corresponding value of 87.4% in N_2. In contrast, success of the final double-bond conversion using the TX/EDB reference was only at 58.7% in air, and it was enhanced to 67.8% when the sample was protected by N_2. Oxygen inhibition was much more significant when TX/EDB was used as the photo-initiator than when F_2-POSS-$(SH)_4$-TX/EDB was used. When photo-polymerization was initiated by TX/EDB in air, we found that the sample surface was slightly tacky even after 10 min of UV irradiation, which was also confirmed by subsequent atomic force microscopy (AFM) analysis. This result was attributed to oxygen inhibition because of O_2 diffusion from the air. When photo-polymerization of A-BPE-10 was initiated by F_2-POSS-$(SH)_4$-TX/EDB in air, the sample surface was cured using thiol–ene photo-polymerization, which prevented the penetration of O_2 from the air into the sample and consequently reduced oxygen inhibition. Note that the final conversion percentage for initiation using F_2-POSS-$(SH)_4$-TX/EDB (85.4%) in air was still much higher than that when TX/EDB was used as an initiator in N_2 (67.8%). The high efficiency of F_2-POSS-$(SH)_4$-TX/EDB was attributed to the presence of the thiol groups and the intramolecular hydrogen abstraction between TX and EDB, which facilitates the generation of free radicals under exposure to UV light.

The self-assembly of F_2-POSS-$(SH)_4$-TX/EDB in the top layer to form a physical barrier was confirmed by depth-dependent X-ray photo-electron spectroscopy (XPS). The strong signal related to F 1s (**Figure 2**) was found in the XPS spectra of the surface, and the corresponding fluorine content was close to that of F_2-POSS-$(SH)_4$-TX/EDB and much higher than that of the entire photo-cured system, suggesting that F_2-POSS-$(SH)_4$-TX/EDB aggregated on the surface. The relative fluorine content to carbon (F/C) changed slightly as analysis went deeper into the film from 0 to 720 nm from the surface, and it decreased dramatically at a depth of approximately 1200 nm. The driving force for the migration of F_2-POSS-$(SH)_4$-TX/EDB to the surface was attributed to the interface energy between air and liquid A-BPE-10. The XPS results for the depth-dependent

fluorine content indicated the presence of two layers: most of the F_2-POSS-$(SH)_4$-TX/EDB migrated to the surface to form a top layer rich in nano-photo-initiator, which was 720- to 1200-nm thick, whereas a small portion of the F_2-POSS-$(SH)_4$-TX/EDB dissolved in the bulk layer of A-BPE-10. In contrast to the gradient distribution of 1173-F in the acrylate monomer in Nie and co-worker's system,[21] the self-assembly of F_2-POSS-$(SH)_4$-TX/EDB at the air/liquid interface formed a top layer resulting from the super-low surface energy of fluorinated POSS and the nature of the F_2-POSS-$(SH)_4$-TX/EDB nanoparticles.[25,27] The high content of the photo-initiator moieties TX/EDB and the thiol groups enabled the top layer to be cured via thiol–ene photo-polymerization even when the sample was exposed to air; this high content was a key factor for reducing oxygen inhibition and achieving a high percentage of final double-bond conversion.

To further confirm the aggregation of F_2-POSS-$(SH)_4$-TX/EDB at the air/(monomer liquid) interface, AFM was used to examine the surface mechanical properties of the A-BPE-10 films containing F_2-POSS-$(SH)_4$-TX/EDB and TX/EDB (as a reference); the films were photo-cured under N_2 for protection or exposed to air. The Young's modulus (E) of the film was calculated from the AFM force curves (Figure 2b). The surface Young's modulus for the films that were formed with F_2-POSS-$(SH)_4$-TX/EDB as an initiator and with photo-curing in N_2 or air were 516 and 499 MPa, respectively; these values are much higher than the corresponding value of 24 MPa for the film that was formed with TX/EDB as the photo-initiator and with photo-curing under N_2. The higher surface moduli of the films produced using F_2-POSS-$(SH)_4$-TX/EDB as photo-initiator resulted from the aggregation of the F_2-POSS-$(SH)_4$-TX/EDB nano-photo-initiators at the air/liquid interface, which formed a hybrid top layer containing POSS. The incorporation of inorganic POSS generally enhances the mechanical performance of photo-cured films. The Young's moduli for the films that were photo-cured in N_2 and in air were almost identical, indicating that O_2 inhibition had no obvious effect on the photo-curing of the film for which F_2-POSS-$(SH)_4$-TX/EDB was used as a photo-initiator. In contrast, the film for which TX/EDB was used as a photo-initiator and for which photo-curing occurred in air exhibited a lower Young's modulus (16 MPa) than that (24 MPa) of the film that was photo-cured in N_2, suggesting that the top layer of the film photo-cured in air was not completely cross-linked. Detailed information can be obtained from the AFM curves. Figure 2b shows that the photo-cured films for which TX/EDB was used as a photo-initiator exhibited a sharp decrease in the force prior to actual contact, and a clearly negative force was required to retract the tip from the sample surface because of the strong adhesion between the AFM tip and the film.[28] Similar behavior was not observed when F_2-POSS-$(SH)_4$-TX/EDB was used as a photo-initiator for the films. The much lower adhesive force for the photo-cured films that were formed using F_2-POSS-$(SH)_4$-TX/EDB as a photo-initiator was attributed to two factors: the lowering of the surface energy of the top layer because of the aggregation of fluorocarbon chains containing F_2-POSS-$(SH)_4$-TX/EDB at the air/film interface and the increase in the degree of cross-linking that was induced by the higher percentage of double-bond conversion. These results from AFM force curves were in good agreement with the results of the XPS analyses and supported our hypothesis that F_2-POSS-$(SH)_4$-TX/EDB nano-photo-initiators can self-assemble at an air/(monomer liquid) interface to form a cross-linked top layer via thiol–ene photo-polymerization, thereby creating a physical barrier to oxygen inhibition.

To further understand the function of the fluorocarbon chains, thiol groups, and photo-initiator moieties of TX/EDB in F_2-POSS-$(SH)_4$-TX/EDB, we designed three additional model photo-initiator systems as reference cases and investigated their photo-polymerization kinetics (**Figure 3**). Unlike the physical mixture of F_2-POSS-$(SH)_6$ and TX/EDB (labeled as F_2-POSS-$(SH)_6$@TX/EDB), TX and EDB photo-initiator moieties were chemically grafted onto the POSS skeleton in F_2-POSS-$(SH)_4$-TX/EDB. B_2-POSS-$(SH)_4$-TX/EDB was designed without fluorinated carbon chains to determine the effect of the fluorocarbon chains, and F_2-POSS-B_4-TX/EDB was used to investigate the effect of the thiol groups (Figure 3a). 'B' in these systems represents a butylthio chain. Photo-polymerization experiments of A-BPE-10 using these photo-initiator systems were carried out in N_2 and in air. Figure 3b shows that the use of F_2-POSS-$(SH)_4$-TX/EDB resulted in the highest percentage of final double-bond conversion among these photo-initiator systems in N_2 and in air.

The final double-bond conversion for the sample with F_2-POSS-$(SH)_6$@TX/EDB was much lower than that of F_2-POSS-$(SH)_4$-TX/EDB, which may have resulted from F_2-POSS-$(SH)_6$@TX/EDB being a physical mixture. In the physical mixture of TX/EDB and F_2-POSS-$(SH)_6$, the migration of fluorinated POSS to the air/film interface did not promote the aggregation of photo-initiator moieties TX/EDB in the top layer, resulting in a relatively low photo-initiation efficiency. Note that the double-bond conversion of the sample containing TX/EDB was enhanced by the addition of F_2-POSS-$(SH)_6$, which promoted thiol–ene photo-polymerization. Using B_2-POSS-$(SH)_4$-TX/EDB with butylthio chains instead of fluorocarbon chains was less efficient than using F_2-POSS-$(SH)_4$-TX/EDB for the photo-polymerization of A-BPE-10. The final double-bond conversion with B_2-POSS-$(SH)_4$-TX/EDB clearly increased from 71.2% in air to 81.7% in N_2. This result was attributed to the absence of aggregation of B_2-POSS-$(SH)_4$-TX/EDB at the air/film interface because of the absence of low-surface-energy fluorocarbon chains in B_2-POSS-$(SH)_4$-TX/EDB. The higher efficiency of B_2-POSS-$(SH)_4$-TX/EDB compared to TX/EDB indicates that thiol groups offer an advantage in the photo-polymerization of acrylate. Although F_2-POSS-B_4-TX/EDB can aggregate on the top layer as F_2-POSS-$(SH)_4$-TX/EDB, the percentage of final double-bond conversion for the sample containing F_2-POSS-B_4-TX/EDB was less than that of the sample containing F_2-POSS-$(SH)_4$-TX/EDB. This result was attributed to the absence of thiol groups, which resulted in conventional radical photo-polymerization instead of oxygen-insensitive thiol–ene photo-polymerization in the top layer for the sample containing F_2-POSS-B_4-TX/EDB. These results from the different model photo-initiator systems show that the synergistic effect of functional groups in the F_2-POSS-$(SH)_4$-TX/EDB nano-photo-initiator, i.e., fluorocarbon chains, thiol groups, and the TX/EDB photo-initiator moieties, played a critical role in preventing oxygen inhibition.

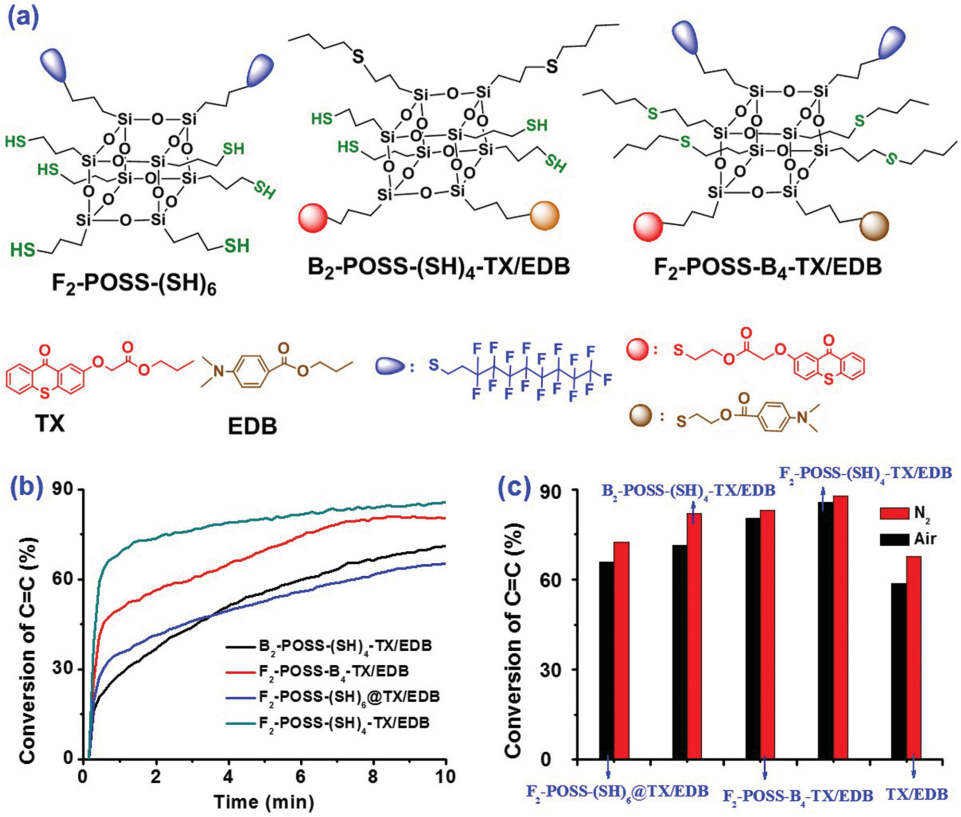

Figure 3. a) Chemical structure of model photo-initiator systems. b,c) Percentage of final double-bond conversion with respect to time (b) and to compare the polymerization of A-BPE-10 initiated by F_2-POSS-$(SH)_4$-TX/EDB, B_2-POSS-$(SH)_4$-TX/EDB, F_2-POSS-B_4-TX/EDB, and F_2-POSS-$(SH)_6$@TX/EDB in air and in N_2 (c). All of the photo-initiator concentrations were 0.0248 M in terms of the TX moiety; the light intensity was 3 mW cm^{-2}, and the exposure time was 10 min.

We verified the feasibility of using F_2-POSS-$(SH)_4$-TX/EDB as a nano-photo-initiator to prevent oxygen inhibition by investigating the photo-polymerization of four common multi-acrylate monomers—polyethylene glycol diacrylate (PEGDA), poly(propylene glycol) diacrylate (PPGDA), trimethylolpropane triacrylate (TMPTA), and 1,6-hexanediol diacrylate (HDDA)—using F_2-POSS-$(SH)_4$-TX/EDB and TX/EDB as initiators in N_2 and in air (**Figure 4**). As in the photo-polymerization of A-BPE-10, F_2-POSS-$(SH)_4$-TX/EDB initiated the photo-polymerization of PEGDA, PPGDA, TMPTA, and HDDA very efficiently in air. Under the same photo-curing conditions, the percentages of final double-bond conversions for the samples containing F_2-POSS-$(SH)_4$-TX/EDB were much higher than those of samples for which TX/EDB was used as a photo-initiator. Moreover, the photo-polymerization behavior of the samples containing F_2-POSS-$(SH)_4$-TX/EDB that were exposed to air were similar to those of the samples that were protected by N_2, suggesting that F_2-POSS-$(SH)_4$-TX/EDB prevented oxygen inhibition in the photo-polymerization of these four acrylate monomers.

There are two critical processes in our strategy to prevent oxygen inhibition: the formation of a top layer via the self-assembly of F_2-POSS-$(SH)_4$-TX/EDB at the air/liquid interface and the oxygen-insensitive thiol–ene photo-polymerization in the top layer, which is further supported by the generation of a wrinkled pattern. To decrease the air/liquid interface energy, F_2-POSS-$(SH)_4$-TX/EDB can migrate to the surface and self-assemble into the top layer. Upon exposure to UV light, thiol–ene photo-polymerizes in the top layer, while conventional radical polymerization proceeds in the bulk layer. The different shrinkage rates after polymerization and the mismatch in the Young's modulus between the top and bulk layers can produce a compressive stress that triggers buckling, resulting in the simultaneous formation of a complex wrinkled pattern.[29–31] Vogt and co-workers reported that the surface segregation of a photo-catalyst produced a mismatch in the polymerization rates between the top and bottom layers of furfuryl alcohol, creating a substantial compressive stress between the bilayers that generated surface wrinkles.[30] However, our system was different from that of Vogt's system in some cases; our fluorinated nano-photo-initiators self-assembled on the top layer of an acrylate liquid resin, which exhibited a concentration gradient from the top to bottom layer, causing different types of reactions to occur between the two layers. Oxygen-insensitive thiol–ene photo-polymerization occurred in the top layer of the acrylate liquid resin, while conventional free radical photo-polymerization proceeded in the bottom layer in the absence of thiol groups. The mismatch in the shrinkage and modulus between the bilayers that was induced by different types and rates of photo-cross-linking reactions generated a self-wrinkled pattern.[23] This process was observed for photo-cured films with a wrinkled pattern, for which F_2-POSS-$(SH)_4$-TX/EDB was used as a photo-initiator. Scanning electron microscopy (SEM)

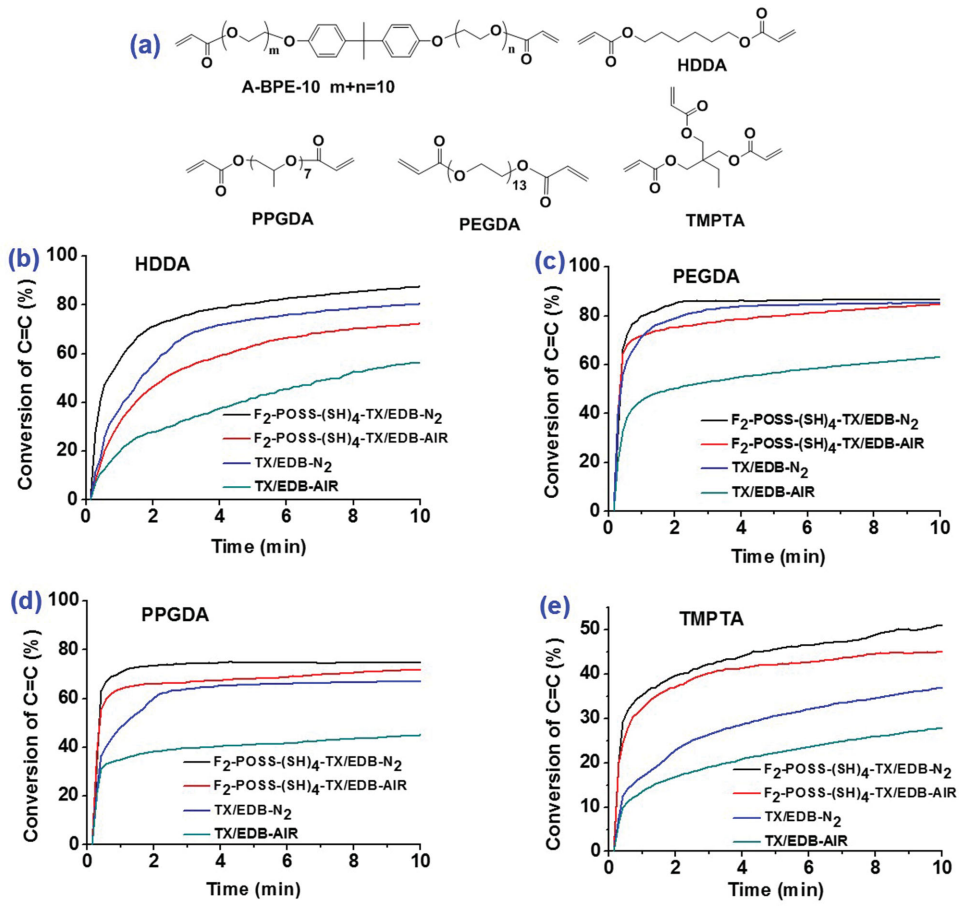

Figure 4. a) Chemical structure of acrylate monomers. b–e) photo-polymerization kinetics of HDDA (b), PEGDA (c), PPGDA (d), and TMPTA (e) in N_2 and in air; F_2-POSS-$(SH)_4$-TX/EDB and TX/ED were used as photo-initiators at concentrations of 0.0248 M in terms of TX moieties at a light intensity of 3 mW cm^{-2}.

and AFM were used to determine the surface morphology, considering the A-BPE-10 and HDDA samples as examples. **Figure 5** shows the typical wrinkled patterns that were observed in the SEM and AFM images for samples in which F_2-POSS-$(SH)_4$-TX/EDB was used as a photo-initiator. In contrast, no pattern was found for the reference sample in which TX/EDB was used as a photo-initiator (Figure S8, SI), which can be explained by the absence of a bilayer structure in this sample. TX/EDB did not aggregate at the air/(liquid monomer) interface to form the top layer; thus, no wrinkled pattern was formed. The difference in the surface morphologies of the A-BPE-10 and HDDA samples could be attributed to the difference in the photo-curing systems under consideration.[23] Note that the self-wrinkled pattern existed at the microscale and thus did not affect the appearance of the photo-cured film. The photo-cured films with a wrinkled pattern appeared smooth and transparent to the naked eye (Figure S9, SI).

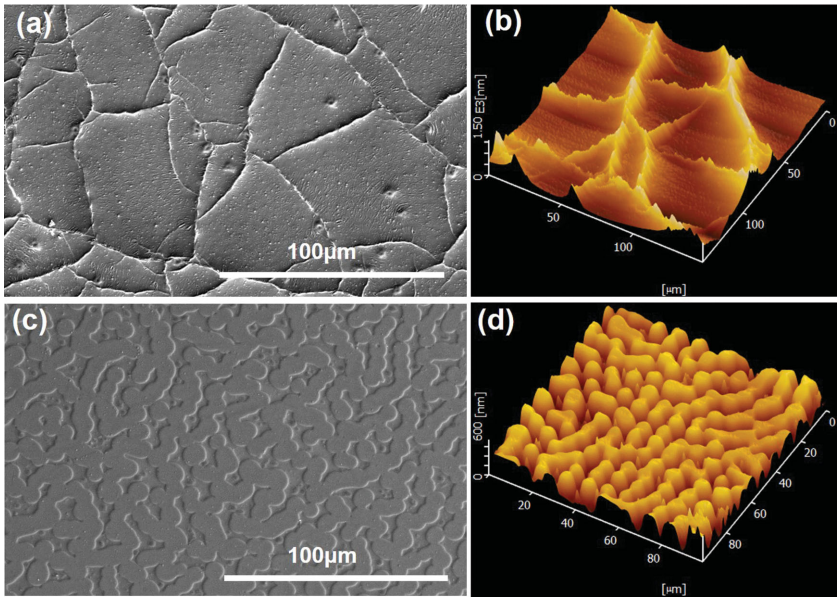

Figure 5. a,c) SEM and b,d) AFM images of photo-cured A-BPE-10 (a,b) and HDDA films (c,d); the concentration of the F_2-POSS-$(SH)_4$-TX/EDB photo-initiator was 0.041 M in terms of the TX moiety, and the intensity and exposure time of UV light were 3 mW cm^{-2} and 10 min, respectively.

The wrinkled pattern of A-BPE-10 is similar to the venation network pattern of a leaf. Kim et al. reported a wrinkled pattern similar to that of a leaf on the elastic film of a bilayer under biaxial compressive stress.[31] Stress-release mechanisms could be important in generating this bio-mimetic pattern. In our strategy, the formation of a self-wrinkled pattern results from the self-assembly of chemical species and photo-polymerization; thus, this "bottom-up" approach may provide an alternative that is similar to biological processes to fabricate a biomimetic patterned surface.

Generally, the use of fluorinated POSS to both coat surfaces[23,25] and produce a wrinkled pattern[32,33] has a significant effect on the wettability of the coated surface. Complex micro- and nano-patterned surfaces in nature, such as the lotus leaf, can result in unique functions such as self-cleaning[33] and superhydrophobicity.[34] The surface of our wrinkled film possesses similar characteristics to complex patterned surfaces in nature. This observation motivated us to investigate the wettability of the wrinkled patterned surface by measuring the water contact angle (WCA) and the di-iodomethane contact angle (DCA). The data from the WCA measurements and the surface energy that was calculated from the WCA and DCA are shown in **Figure 6**. Using F_2-POSS-$(SH)_4$-TX/EDB as the photo-initiator significantly enhanced the WCA values for the A-BPE-10 and HDDA samples and clearly lowered the surface energy compared to the corresponding values for the samples in which TX/EDB was used as the photo-initiator. For example, using F_2-POSS-$(SH)_4$-TX/EDB as the photo-initiator increased the WCA for A-BPE-10 from 50° to 100° and decreased the surface energy from 53 to 22 mN m^{-1}. The contact angle value was lower than that obtained in our previous study,[23] which may have resulted from the absence of nanowrinkled patterns in this study. The substantial hydrophilicity of the cross-linker substrate prevented the wettability of our surface with the wrinkled pattern from exceeding that in other reports;[32,34] however, the surface properties of the resulting resins, such as the wettability and rigidity, were clearly improved because of the use of the fluorinated POSS and the wrinkled pattern on the coated surfaces. The photo-cured film for which F_2-POSS-$(SH)_4$-TX/EDB was used as an initiator had a relatively low surface energy, suggesting that the film was self-cleaning because of the combination of the micropatterned morphology and the fluorocarbon chain coverage. A similar phenomenon was also found for the HDDA film in which F_2-POSS-$(SH)_4$-TX/EDB was used as the photo-initiator.

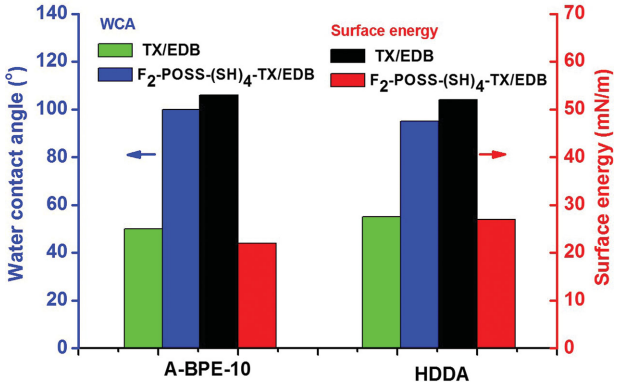

Figure 6. Water contact angle (WCA) and surface energy of photo-cured A-BPE-10 and HDDA films. The concentration of the F_2-POSS-$(SH)_4$-TX-EDB photo-initiator was 0.041 M in terms of the TX moiety, and the intensity and exposure time of UV light were 3 mW cm^{-2} and 10 min, respectively.

3. Conclusion

In summary, we have demonstrated that using multi-functional F_2-POSS-$(SH)_4$-TX/EDB as a nano-photo-initiator can significantly reduce oxygen inhibition in the photo-polymerization of various acrylate monomers. F_2-POSS-$(SH)_4$-TX/EDB consisted of a thiol-containing polyhedral oligomeric silsesquioxane (POSS) skeleton onto which fluorocarbon chains and thioxane/dimethylaminobenzoate (TX/EDB) photo-initiator moieties were grafted. F_2-POSS-$(SH)_4$-TX/EDB self-assembled at the interface between air and the liquid monomer and formed a cross-linked top layer via thiol–ene polymerization, which served as a physical barrier to the diffusion of oxygen from the surface into the bulk layer. Furthermore, a self-wrinkled pattern was obtained because of the mismatch in the shrinkage between the top and bulk layers that resulted from the different types of photo-cross-linking reactions. We expect this strategy—in which the self-assembly of multifunctional nano-photo-initiators at the air/liquid interface prevents oxygen inhibition and creates a self-wrinkled pattern—to find wide application in photo-curing technology.

4. Experimental Section

Preparation of Photo-Cured Samples: In the preparation of films for measurements, the photo-initiator concentration was expressed in terms of the TX moiety. Acrylate monomer (1.0 g) and a certain amount of photo-initiator were dissolved in chloroform (1 mL) by stirring. The as-prepared resin mixture with a fixed mass was drop-coated onto an infrared transmitting silicon wafer or a glass slide. The sample was maintained at 60 °C for 30 min to remove the solvent and then photo-cured by irradiation with 365-nm UV light (using a light-emitting diode (LED) with an intensity of approximately 10 mW cm^{-2}) for the desired time.

Measurements: The photo-polymerization kinetics were traced using real-time FT-IR, which was recorded from 4000 to 400 cm^{-1} at a 4 cm^{-1} resolution on a Spectrum 100 FT-IR absorption spectrometer (Nicolet IS10).[35] The conversions were calculated from the ratio of the peak area after polymerization to that before polymerization.

The AFM images were obtained using a scanning probe microscope (Nanoscope III, Digital Instruments) that was operated in tapping mode with silicon cantilevers (with a force constant of 40 $N{\cdot}m^{-1}$). The force curves were collected in contact-mode AFM using silicon cantilevers with a spring constant of 3 $N{\cdot}m^{-1}$; ten force curves were recorded for each example. The Young's modulus (E) was calculated as the average value of the approach and the retraction traces for each force curve using the Hertz model. The measurement of the E using AFM is described in detail in the SI.

SEM was performed using a Sirion-200 electron microscope (FEI Company) at 5 kV. The contact angle measurements were recorded using a spinning drop interface tensiometer (SL200C, USA KINO Industry). XPS experiments were carried out on a PHI-5000C ESCA system (Perkin-Elmer) with Al Kα radiation ($h\nu$ = 1486.6 eV). Generally, the X-ray anode was run at 250 W, and the high voltage was maintained at 14.0 kV with a detection angle of 54°. The pass energy was fixed at 46.95 eV to ensure

sufficient sensitivity. The base pressure of the analyzer chamber was approximately 5×10^{-8} Pa.

Supporting Information

Supporting Information is available from the Wiley Online Library or from the author.

Acknowledgements

The authors thank the National Basic Research Program (2013CB834506), the National Nature Science Foundation of China (21174085, 21274088, 51373098), the Education Commission of Shanghai Municipal Government (12ZZ020), and the Shanghai Key Lab of Polymer and Electrical Insulation for their financial support. X. J. is supported by the NCET-12–3050 Project.

Received: August 21, 2014
Revised: October 1, 2014
Published online:

[1] J. P. Fouassier, Photoinitiation, Photopolymerization and Photocuring: *Fundamental and Applications,* Hanser Publishers, New York, NY **1995**.
[2] R. Schwalm, UV Coatings-Basics, *Recent Developments and New Applications*, 1st ed., Elsevier, Amsterdam, The Netherlands **2007**.
[3] C. Decker, *Macromol. Rapid Commun.* **2002**, *23*, 1067.
[4] H. Benjamin, D. William, G. Giulia, D. Fazzi, F. Brandi, A. Petrozza, A. Diaspro, *Adv. Mater.* **2013**, *25*, 904.
[5] H. Lu, J. W. Stansbury, J. Nie, A. K. Berchtold, C. N. Bowman, *Biomaterials* **2005**, *26*, 1329.
[6] Y. Yusuf, J. Steffen, J. T. Nicholas, *Macromolecules* **2010**, *43*, 6245.
[7] E. Peris, M. J. Banüls, A. Maquieira, R. Puchades, *Trends Anal. Chem.* **2012**, *41*, 86.
[8] V. A. Bhanu, K. Kishore, *Chem. Rev.* **1991**, *91*, 99.
[9] A. V. Fedorov, A. A. Ermoshkin, A. Mejiritski, D. C. Neckers, *Macromolecules* **2007**, *40*, 3554.
[10] S. C. Ligon, B. Husár, H. Wutzel, R. Holman, R. Liska, *Chem. Rev.* **2014**, *114*, 557.
[11] C. Decker, A. D. Jenkins, *Macromolecules* **1985**, *18*, 1241.
[12] N. B. Cramer, C. N. Bowman, *J. Polym. Sci. A: Polym. Chem.* **2001**, *39*, 3311.
[13] N. B. Cramer, J. P. Scott, C. N. Bowman, *Macromolecules* **2002**, *35*, 5361.
[14] A. K. O'Brien, N. B. Cramer, C. N. Bowman, *J. Polym. Sci. A: Polym Chem.* **2006**, *44*, 2007.
[15] M. A. Tehfe, S. Mondal, M. Nechab, F. Dumur, M. P. Bertrand, B. Graff, D. Gigmes, J. P. Fouassier, J. Lalevée, *Macromol. Chem. Phys.* **2013**, *214*, 1302.
[16] a) J. Lalevée, M. A. Tehfe, X. Allonas, J. P. Fouassier, *Macromolecules* **2008**, *41*, 9057; b) J. Lalevee, S. Telitel, M. A. Tehfe, J. P. Fouassier, D. P. Curran, E. Lacote, *Angew. Chem. Int. Ed. Engl.* **2012**, *51*, 5958; c) E. R. Mohamad, J. Lalevée, X. Allonas, J. P. Fouassier, *Macromolecules* **2009**, *42*, 8725; d) J. Lalevee, A. Dirani, M. El-Roz, X. Allonas, J. P. Fouassier, *Macromolecules* **2008**, *41*, 2003.
[17] a) J. Lalevée, N. Blanchard, A. C. Chany, M. El-Roz, R. Souane, B. Graff, X. Allonas, J. P. Fouassier, *Macromolecules* **2009**, *42*, 6031; b). J. Lalevee, J. P. Fouassier, *Polym. Chem.* **2011**, *2*, 1107.
[18] a) M. Höfer, N. Moszner, R. Liskar, *J. Polym. Sci. A: Polym. Chem.* **2008**, *46*, 6916; b) R. Shenoy, C. N. Bowman, *Macromolecules* **2010**, *43*, 7964; c) C. Belon, X. Allonas, C. Croutxe-Barghorn, J. Lalevée, *J. Polym. Sci. A: Polym. Chem.* **2010**, *48*, 2462; d) O. Faruk, U. K. Muhammet, Y. Yusuf, *J. Polym. Sci. A: Polym. Chem.* **2013**, *51*, 1685.
[19] a) N. B. Cramer, C. P. O'Brien, C. N. Bowman, *Polymer* **2008**, *49*, 4756; b) C. E. Corcione, M. Frigione, *Thermochim. Acta* **2012**, *534*, 21; c) M. Awokola, W. Lenhard, H. Löffler, C. Flosbach, P. Frese, *Prog. Org. Coat.* **2002**, *44*, 211; d) T. Ranjan, V. C. James, F. Rudolf, *J. Polym. Sci. A: Polym. Chem.* **2013**, *51*, 305.
[20] a) D. K. Balta, N. Arsu, Y. Yagci, S. Jockusch, N. J. Turro, *Macromolecules* **2007**, *40*, 4138; b) D. K. Balta, N. Arsu, Y. Yagci, A. K. Sundaresan, S. Jockusch, N. J. Turro, *Macromolecules* **2011**, *44*, 2531; c) D. L. Versace, F. Dalmas, J. P. Fouassier, J. Lalevée, *ACS. Macro. Lett.* **2013**, *2*, 341.
[21] F. Xu, J. L. Yang, Y. S. Gong, G. P. Ma, J. Nie, *Macromolecules* **2012**, *45*, 1158.
[22] K. Studer, C. Decker, E. Beck, R. Schwalm, *Prog. Org. Coat.* **2003**, *48*, 92.
[23] Y. C. Gan, X. S. Jiang, Y. Jie, *Macromolecules* **2012**, *45*, 7520.
[24] a) C. E. Hoyle, T. Y. Lee, T. Roper, *J. Polym. Sci.: Polym. Chem.* **2004**, *42*, 5301; b) A. K. O'Brien, N. B. Cramer, C. N. Bowman, *J. Polym. Sci. A: Polym. Chem.* **2006**, *44*, 2007; c) K. L. Killops, L. M. Campos, C. J. Hawker, *J. Am. Chem. Soc.* **2008**, *130*, 5062; d) L. M. Campos, I. Meinel, R. G. Guino, M. Schierhorn, N. Gupta, G. D. Stucky, C. J. Hawker, *Adv. Mater.* **2008**, *20*, 3728; e) C. N. Bowman, C. E. Hoyle, *Angew. Chem. Int. Ed.* **2010**, *49*, 1540.
[25] a) K. Koh, S. Sugiyama, T. Morinaga, K. Ohno, Y. Tsujii, T. Fukuda, M. Yamahiro, T. Iijima, H. Oikawa, K. Watanabe, T. Miyashita, *Macromolecules* **2005**, *38*, 1264; b) Y. S. Ye, W. Y. Chen, Y. Z. Wang, *J. Polym. Sci.: Polym. Chem.* **2006**, *44*, 5391; c) A. Tutejaa, W. Choi, J. M. Mabry, G. H. McKinley, R. E. Cohen, *Proc. Natl. Acad. Sci. USA* **2008**, *105*, 18200; d) S. W. Kuo, F. C. Chang, *Prog. Polym. Sci.* **2011**, *36*, 1649; e) W. Zhang, A. H. E. Müller, *Prog. Polym. Sci.* **2013**, *38*, 1121.
[26] a) D. Tunc, Y. Yagci, *Polym. Chem.* **2011**, *11*, 2557; b) S. E. Korkut, G. Temel, D. K. Balta, N. Arsu, M. K. Sener, *J. Lumin.* **2013**, *136*, 389.
[27] a) W. Ming, M. Tian, R. D. van de Grampel, F. Melis, X. Jia, J. Loos, R. van der Linde, *Macromolecules* **2002**, *35*, 6920; b) A. F. Thünemann, A. Lieske, B. R. Paulke, *Adv. Mater.* **1999**, *11*, 321; c) K. Koh, S. Sugiyama, T. Morinaga, K. Ohno, Y. Tsujii, T. Fukuda, M. Yamahiro, T. Iijima, H. Oikawa, K. Watanabe, T. Miyashita, *Macromolecules* **2005**, *38*, 1264.
[28] M. Guvendiren, S. Yang, J. A. Burdick, *Adv. Funct. Mater.* **2009**, *19*, 3038.
[29] C. M. Chen, S. Yang, *Polym. Int.* **2012**, *61*, 1041.
[30] J. M. Torres, C. M. Stafford, B. D. Vogt, *Soft Matter* **2012**, *8*, 5225.
[31] P. Kim, M. Abkarian, H. A. Stone, *Nat. Mater.* **2011**, *10*, 952.
[32] a) J. Y. Chung, J. P. Youngblood, C. M. Stafford, *Soft Matter* **2007**, *3*, 1163; b) S. Yang, K. Khare, P. C. Lin, *Adv. Funct. Mater.* **2010**, *20*, 2550; c) Y. H. Kim, Y. M. Lee, J. Y. Lee, M. J. Ko, P. J. Yoo, *ACS Nano* **2012**, *6*, 1082; d) S. G. Lee, H. S. Lim, D. Y. Lee, D. Kwak, K. Cho, *Adv. Funct. Mater.* **2013**, *23*, 547; e) A. Milionis, R. Giannuzzi, I. S. Bayer, E. L. Papadopoulou, R. Ruffilli, M. Manca, A. Athanassiou, *ACS Appl. Mater. Interfaces* **2013**, *5*, 7139; f) U. Manna, M. C. D. Carter, D. M. Lynn, *Adv. Mater.* **2013**, *25*, 3085.
[33] A. Lafuma, D. Quere, *Nat. Mater.* **2003**, *2*, 457.
[34] K. C. Park, H. J. Choi, C. H. Chang, R. E. Cohen, G. H. Mckinley, G. Barbastathis, *ACS Nano* **2012**, *6*, 3789.
[35] Y. L. Xu, H. L. Xu, X. S. Jiang, J. Yin, *Adv. Funct. Mater.* **2014**, *24*, 1679.